

Adsorption Kinetics and Isotherm of Crystal Violet by Carbon Modified with Magnetite (Fe₃O₄) and Triethoxyphenylsilane (TEPS) from Rubber Fruit Shell

Nadya Syarifatul Fajriyah¹, Buhani Buhani^{2*}, and Suharso Suharso²

¹Postgraduate Student of Master Program in Chemistry, Department of Chemistry, University of Lampung, Jl. Sumantri Brojonegoro No 1, Bandar Lampung 35145, Indonesia

²Department of Chemistry, Faculty of Mathematics and Natural Sciences, University of Lampung, Jl. Sumantri Brojonegoro No. 1, Bandar Lampung 35145, Indonesia

* **Corresponding author:**

tel: +62-81278152368

email: buhani_s@yahoo.co.id

Received: July 13, 2022

Accepted: September 30, 2022

DOI: 10.22146/ijc.76201

Abstract: Rubber fruit shells-derived carbon (RC) modified with magnetite (MRC) and triethoxyphenylsilane (TEPS) (SRC) made from rubber fruit shells were used to adsorb crystal violet (CV) dye effectively. The RC was successfully modified by magnetite and TEPS, according to the characterization of the adsorbent utilizing Fourier transform infrared (FTIR) spectroscopy, X-ray diffraction (XRD), and scanning electron microscopy-energy-dispersive X-ray (SEM-EDX) showed that the RC was successfully modified by magnetite and TEPS. Several adsorption process parameters were investigated, and the ideal results were obtained with an adsorbent dose of 0.1 g, pH 10, contact time of 15 min, and initial concentration of CV 250 mg L⁻¹. The MRC and SRC adsorption capacities are 71.43 and 69.93 mg g⁻¹, respectively. The adsorption kinetics followed a pseudo-second-order model with MRC and SRC rate constants of 3.40 and 0.83 g mg⁻¹ min⁻¹, respectively. The Freundlich adsorption isotherm is suitable for CV dye adsorption using MRC and SRC with K_F values are 1.36 and 1.76 mg g⁻¹ L mg⁻¹ which gives R² 0.943 and 0.932, respectively. These findings showed that the modified RC with magnetite and TEPS effectively removes the CV dye solution through the adsorption process.

Keywords: magnetite rubber fruit shells-derived carbon; silane rubber fruit shells-derived carbon; adsorption; crystal violet; rubber fruit shells

■ INTRODUCTION

Environmental issues, especially in Indonesia, are still a problem that needs attention. Various residual pollutants from human activities interfere with the life processes of living things, especially water pollution. Water is said to be polluted when it cannot be used according to its function. Water pollution commonly found can be in the form of dyes, herbicides, heavy metals, and other contaminants that accumulate in the environment [1].

One of the most common industrial pollutants is the textile industry. The textile industry produces a lot of dye waste in the environment. Dyes used in the textile industry are classified into three categories, namely cationic, anionic, and non-ionic dyes [2-3]. Cationic dyes are hazardous compared to others and are most widely

used in the textile industry. Crystal violet (CV) is triphenylmethane and one of the cationic dyes used in various industries, such as pharmaceuticals, paper, textiles, and printer inks [4]. CV, if getting in the water even with just a minor concentration of 1 ppm, can reduce the penetration of sunlight and interfere with the photosynthesis process [5]. If CV enters the human body a certain amount, it can cause various diseases such as respiratory problems, eye, and skin irritation, increased heart rate, blindness, and mutagenesis [6]. Considering the impact caused by the presence of CV dye can be harmful to humans, several steps to reduce or even eliminate CV dye waste have been carried out, such as chemical degradation, adsorption, coagulation, filtration membrane, ion exchange, and photocatalysis [6-11].

Adsorption is the cheapest method, easy to do, and proven effective in removing various contaminants, such as dyes, in the aquatic environment [12]. Several adsorbents used to remove CV dyes include organoclay (bentonite-alginate), agricultural waste (pine bark), organic polymers (chitosan composite), biomass (algae), and carbon materials [13-16]. The carbon material is one of the most commonly used adsorbents for the process of adsorption because of its abundant source, good stability, and wide application [17]. In this study, the carbon used came from rubber fruit shells. The rubber fruit shells-derived carbon (RC) was modified using magnetite to overcome the lack of effectiveness of RC. The scientific community has keenly interested in magnetite nanoparticles because of their unique features. Since magnetite has a large surface area and many active surface sites, it has a high capacity for adsorption [18]. The benefit of using magnetic particles is that they may be retrieved by an external magnetic field relatively fast and reused without losing the active site [19-20]. The magnetite-coated material is environmentally safe because it does not produce contaminated substances such as suspended solids. In addition, it enhances the process of removing dyes from the solution [21-22].

The rubber fruit shells-derived carbon magnetite (MRC) has magnetic properties and a more significant molecular weight than ordinary RC, so the filtration process runs more effectively. It is recyclable and doesn't contribute to further environmental issues [23]. Besides, it was modified using magnetite, and modification of RC was also carried out using a triethoxyphenylsilane (TEPS) coupling agent [24]. Silane coupling agent, a silicon-based substance, can improve chemical bonding at the interface of organic and inorganic materials. The silane coupling agent has an R-Si-X₃ structure, where R is an organofunctional group and X is an alkoxy. TEPS is one of the coupling agents that can be applied as a coating to the surface of solid materials because it has two distinct active groups that are linked to silica atoms in the molecule TEPS has a phenyl group that can bind organic materials and an ethoxy group that can bind inorganic materials, which increases the potential of CV dyes to adsorb [24-25].

Therefore, MRC will interact with CV dyes because it has an active group from Fe₃O₄ other than the pores of the RC. The rubber fruit shells-derived carbon silane (SRC) will interact with CV dyes by the phenyl and hydroxyl groups that SRC has. MRC and SRC adsorbents obtained were tested for their ability to CV, covering several parameters, including adsorbent dose, the influence of pH, the influence of contact time, and the concentration of adsorbate. The adsorption kinetics was calculated by converting the data from the contact time parameters into pseudo-first-order and pseudo-second-order equations. The Langmuir and Freundlich equations were used to determine the adsorption isotherm.

■ EXPERIMENTAL SECTION

Materials

Some materials used in this study were CV, FeSO₄·7H₂O, FeCl₃·6H₂O, NaNO₃, HCl, NaOH, ethanol, triethoxyphenylsilane (TEPS) and buffer solution from Merck (Darmstadt Germany). Rubber fruit shells were obtained from East Lampung Regency.

Instrumentation

The adsorbent material was characterized by X-ray diffraction (XRD) (LabX XRD-6000 Shimadzu) to recognize the magnetite's phase after modification, scanning electron microscope-energy-dispersive X-ray (SEM-EDX) (Zeiss EVO MA 10) to discover the surface structure of adsorbents, and FTIR (IRPrestige-21) is used to determine the functional groups of adsorbents. The CV concentration in the solution was determined using UV-Vis Spectrophotometer (Agilent Cary 100).

Procedure

Preparation of RC

Eleven kilograms of rubber fruit shells were cleaned and dried in the sun. Furthermore, it is burned in a drum made of an iron plate with a diameter ± 58 cm and height of 93 cm for approximately 6 h to obtain an RC weighing 3 kg. The RC obtained from carbonization is then pulverized by grinding and sifted through a 100-mesh sieve.

Modification of RC using magnetite coating

The MRC was obtained by putting 6.5 g of RC in 300 mL of distilled water and heating it to 70 °C. Then, iron salt consisting of 7.6 g $\text{FeCl}_3 \cdot 6\text{H}_2\text{O}$ and 3.9 g $\text{FeSO}_4 \cdot 7\text{H}_2\text{O}$ was diffused in 300 mL of distilled water. The mixture was then stirred for 30 min while adding 100 mL of 5 M NaOH dropwise. The obtained residue was separated and neutralized to pH 6. Afterward, it was dried at 100 °C for 3 h [26].

Modification of RC using silane agent TEPS

A total of 4 g of RC was mixed with 200 mL of ethanol. Next, 0.4 mL of triethoxyphenylsilane (TEPS) was put into the mixture and hereafter stirred using a magnetic stirrer for 7 h at 70 °C in a water bath. The resulting SRC was separated and cleansed using ethanol and dried at 60 °C for 1 h [24].

A total of 0.1 g MRC and SRC were put into 20 mL 0.1 M NaNO_3 , respectively. A pH range of 3 to 12 was used for the initial pH. The pH was adjusted by adding 0.1 M HCl and NaOH. Then, the pH was maintained by the addition of a buffer solution. The mixture was stirred using a shaker for 24 h. After that, the final pH was observed and measured using a pH meter [27].

Adsorption experiment

CV adsorption by MRC and SRC was carried out by batch method using several parameters such as adsorbent dose (0.1–0.5 g), solution pH (3–12), contact time (15–120 min), and CV dye concentration (10–250 mg L^{-1}). For each experiment, a certain amount of MRC and SRC were added to 20 mL CV solution with an initial concentration at the appropriate pH value. 0.1 M NaOH and HCl were

used to alter the initial pH solution. At a steady speed of 100 rpm, the mixture was agitated in an orbital shaker. CV residues were analyzed on λ_{max} 590 nm using Spectrophotometer UV-Vis. The CV dye adsorption percentage and adsorption capacity were calculated by Eq. (1) and (2), respectively:

$$\text{Adsorption}(\%) = \frac{C_o - C_e}{C_o} \times 100 \quad (1)$$

$$q = \frac{(C_o - C_e)v}{w} \quad (2)$$

where w (g) is the amount of adsorbent, v (L) is the volume of the solution, q (mg g^{-1}) is the amount of CV dye adsorbed per unit mass, C_o and C_e (mg L^{-1}) are the initial CV concentration and CV concentration after the adsorption, respectively.

RESULTS AND DISCUSSION

Adsorbent Characterization

The MRC modification was carried out through a magnetite coating process using $\text{FeCl}_3 \cdot 6\text{H}_2\text{O}$, and $\text{FeSO}_4 \cdot 7\text{H}_2\text{O}$ mixed to form Fe_3O_4 , which then coats the RC surface. The SRC modification was carried out through the silanization process using a silane coupling agent, namely TEPS. TEPS has two active groups, namely the phenyl group, which can bind organic materials and ethoxy to bind inorganic materials [24].

FTIR characterized the obtained MRC and SRC adsorbents to identify the functional groups, XRD to identify magnetite crystals and SEM-EDX to recognize the RC surface pattern and analyze its constituent elements. Fig. 2 shows a hydroxyl group (OH) as seen by

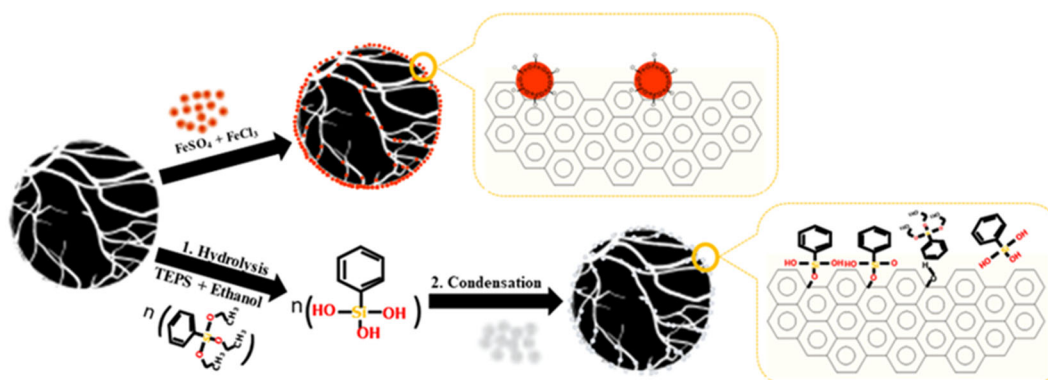


Fig 1. Scheme of RC surface modification using magnetite and silane agent

the peaks at wavenumber 3433 cm^{-1} , and Fe-O is indicated by absorption at wavenumber 586 cm^{-1} which indicates that Fe_3O_4 has coated RC [24].

Peaks at 2368 , 1620 and 1604 cm^{-1} correspond to C-H vibration and the C=C group. Peaks at 1435 and 1527 cm^{-1} correspond to an aromatic C=C group [28-30]. In addition, the presence of Si-O-Si is indicated by the absorption at wavenumber 1049 cm^{-1} which indicates the RC has been coated with TEPS [13].

The XRD pattern (Fig. 3) on the RC shows a broad asymmetric peak at 2θ $20\text{--}45^\circ$, which is characteristic of amorphous carbon. Based on Fig. 3, MRC shows sharp

peaks compared to RC at 2θ 35.46 , 43.04 , 57.22 , and 62.58° [31]. The asymmetrical RC peaks turn into sharp peaks in the XRD MRC pattern, indicating that RC has been coated with magnetite so that the peaks appear with sharp intensity. The SRC diffraction pattern at 2θ $20\text{--}30^\circ$ showed broad peaks, indicating the presence of amorphous silica formed on RC's surface. Amorphous silica was obtained by hydrolysis of TEPS [24].

The morphology of MRC can be seen in Fig. 4(b). The MRC surface looks rougher than the RC surface. Magnetite grains have entirely coated the RC surface. EDX data support this. The elemental compositions of

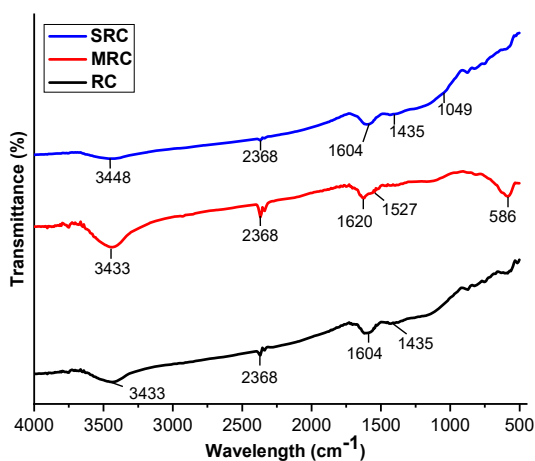


Fig 2. FTIR spectra of RC, MRC, and SRC

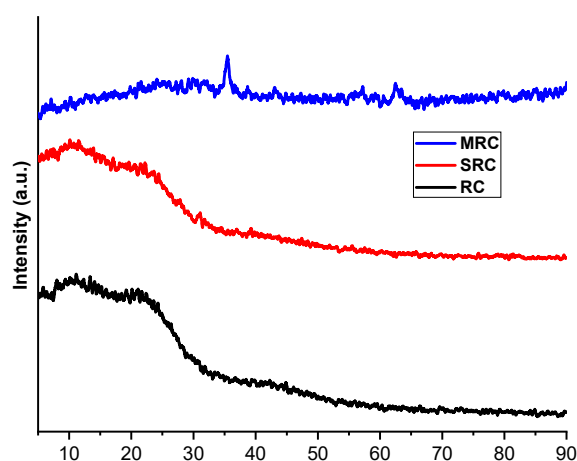


Fig 3. Diffractogram of RC, MRC and SRC

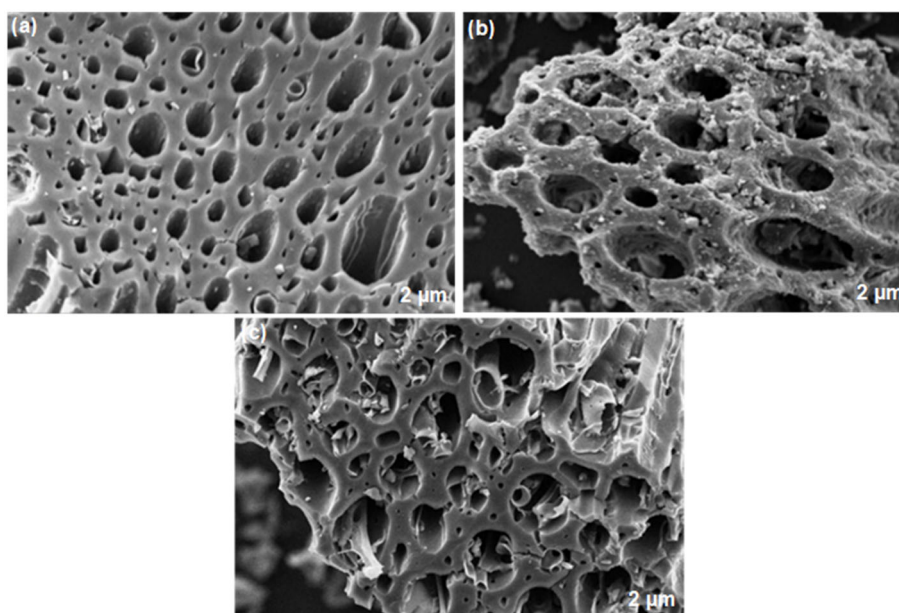


Fig 4. Micrographs of (a) RC, (b) MRC, and (c) SRC

C, O, and Fe are 65.97, 30.95, and 3.08%, respectively.

In addition, the pore diameter of MRC is around 2.05–6.45 μm , smaller than the diameter of RC, which has a pore diameter of around 3.52–9.38 μm . This finding indicates that Fe_3O_4 has been perfectly attached to the RC surface. The particles of Fe_3O_4 coat the entire carbon surface, including the carbon pores, so the carbon pores become narrower, resulting in a smaller carbon pore diameter.

The surface morphology of SRC in Fig. 4(c) shows the presence of small white particles of silica from TEPS modification and stick to the RC pores. Because of the lack of oxygenated surface from RC, TEPS does not

entirely cover the RC pores. The results of the EDX analysis (Fig. 5) showed the elemental compositions of C, O, and Si were 90.43, 9.45, and 0.13%, respectively.

From the EDX data, it can be seen that TEPS has coated the RC surface.

Adsorption Study

Adsorbent dosage

The adsorbent dose can affect the adsorption ability. Fig. 7(a) shows the adsorption percentage depending on the adsorbent dose. Based on Fig. 7(a), the adsorption efficiency decreased while the adsorbent dose increased. This phenomenon is because adsorption

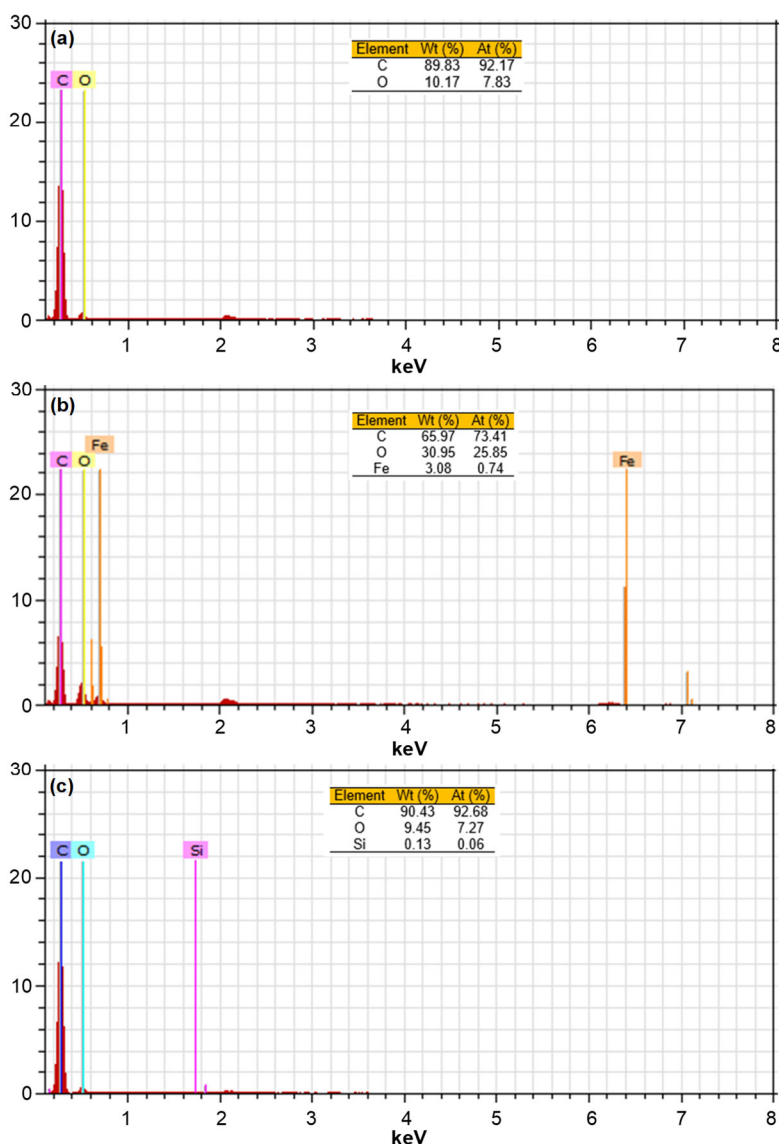


Fig 5. EDX Spectra of (a) RC, (b) MRC and (c) SRC

will occur more quickly as the adsorbent's mass increases. Because of the superficial adsorption, the contact between the adsorbent and adsorbate happens quickly on the adsorbent's surface [32]. The decrease in adsorption efficiency can be due to a decrease in the surface area of the adsorbent so that the adsorbent has reached saturation on its surface. In addition, it can also be caused by overlapping and agglomeration of the large number of adsorbents contained in the adsorbate solution [33]. The optimum mass of the adsorbent in absorbing the CV solution was 0.1 g, with a percent absorption of 92.10% against MRC and 89.59% against SRC.

Influence of pH

The influence of pH depends on the surface charge of the adsorbent and the pH of the adsorbate solution. To determine the surface charge on the adsorbent can be determined by pH_{pzc} . pH_{pzc} is obtained from the difference between the initial pH and the final pH. The surface charge of the adsorbent whose value is close to zero is the optimum zeta potential value of the adsorbent. The surface charge of the adsorbent will be positive if the pH

is below pH_{pzc} and negative if the pH is above pH_{pzc} . The higher the adsorbent surface charge, the lower the pH_{pzc} value or close to zero [34]. The pH_{pzc} values obtained on the MRC and SRC adsorbents were optimum at pH 8 and had a negative surface charge, so they would be good at absorbing positively charged adsorbates (Fig. 6).

As shown in Fig. 7(b), the effect of pH on the CV is insignificant; from pH 4 to 12, the efficiency tends to fluctuate pH 12 at MRC gave the highest adsorption percentage, but the CV solution became saturated. Thus, the optimum pH obtained is pH 10 for both MRC and

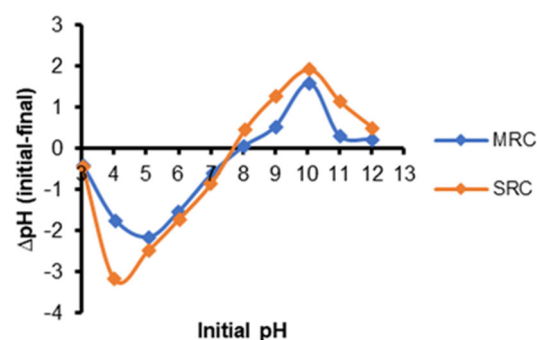


Fig 6. pH_{pzc} curve of MRC and SRC adsorbent

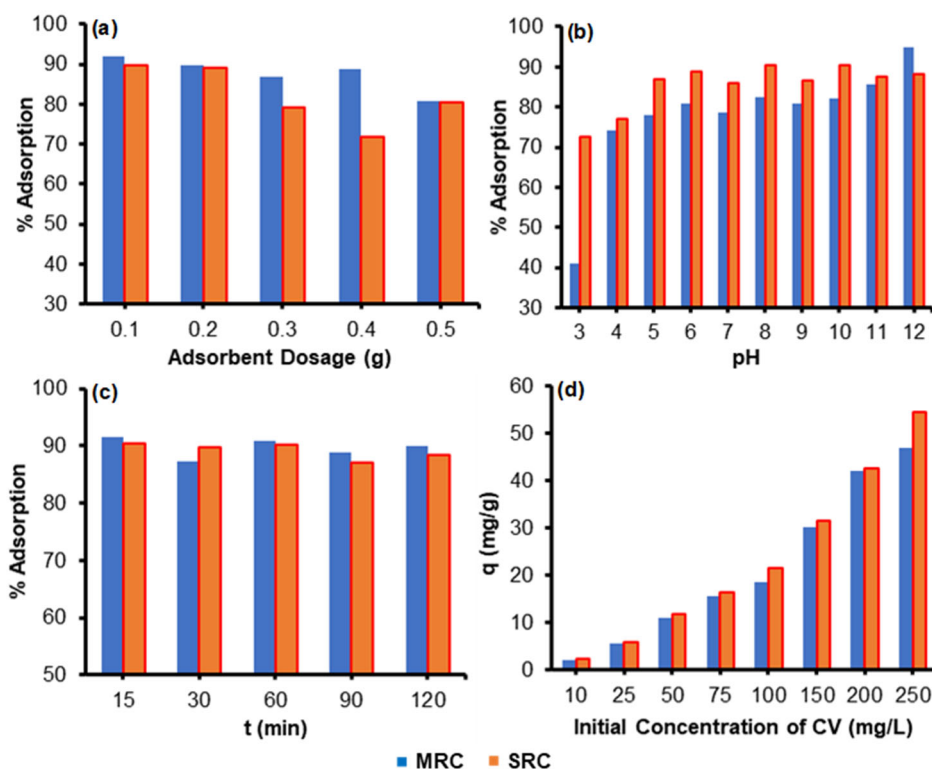


Fig 7. Influence of (a) adsorbent dosage, (b) pH solution, (c) contact time, and (d) initial concentration CV adsorbed by MRC and SRC

SRC, with absorption percentages of 82.15 and 90.37%, respectively. The adsorption percentage obtained indicates that the pH of the solution affects the CV adsorption process, where the results obtained from the SRC adsorbent are better than MRC. This result can occur due to the presence of two active groups in the SRC, which in alkaline conditions gives a more optimal contribution.

At pH 10, the adsorption process worked because it followed the previously obtained pH_{pzc} at pH 8, and the adsorbent had a negative surface charge so that it could interact with a CV which is a cationic dye. Due to competition between CV molecules and H^+ ions on the surface of the adsorbent at $pH < 7$, the adsorption process is not ideal, and a repulsion reaction will occur between the adsorbate and adsorbent [12].

The amount of H^+ ions on the adsorbent's surface will decrease in alkaline conditions ($pH > 7$) so that the adsorbent effectively adsorbs the adsorbate. The more negative the surface charge on the adsorbent, the more electrostatic interactions between the adsorbent and adsorbate will increase. At an increasingly alkaline pH ($pH > 10$), there is an increase in the concentration of OH^- , which will cause precipitation in the solution, and the adsorption ability will be inhibited [35].

Influence of contact time and the kinetic studies

The effect of contact time is essential for defining the appropriate duration for the interaction between adsorbent and adsorbate so that the highest adsorption efficiency may be achieved. Contact time varies from 15 to 120 min. Based on Fig. 7(c), the highest adsorption percentages obtained by MRC and SRC were 91.51 and 90.36%, respectively. Where the results obtained were more remarkable than CV adsorption carried out using Raw *Parthenium hysterophorus* and Raw *Saccharum munja*, which gave the respective adsorption percentages of 84.2 and 86% [36]. The percentage result of adsorption using MRC adsorbent is slightly larger than SRC adsorbent, but the difference is not too significant.

The contact time of 15 min gave the highest efficiency for MRC and SRC adsorbents, which means the adsorption process is faster. This result can occur because of the empty and available part of the surface (active site)

from the adsorbent that can interact with CV dyes. The brief contact time suggests that MRC or SRC with a CV is a physical interaction [37]. The decrease in adsorption efficiency if the contact time is longer can be due to the unavailability or limited availability of active sites on the adsorbent [38]. Thus, the influence of contact time gives a result of 15 min for MRC and SRC to adsorb the CV solution with high efficiency.

The kinetics throughout the adsorption process was computed utilizing the contact time data gathered for this study. Pseudo-first-order and pseudo-second-order kinetics are determined using Eq. (3) and (4), respectively:

$$\ln(q_e - q_t) = \ln(q_e) - k_1 t \quad (3)$$

$$\frac{t}{q_t} = \frac{1}{k_2 q_e^2} + \frac{1}{q_e} t \quad (4)$$

where q_t and q_e ($mg\ g^{-1}$) represent the total adsorption capacity of CV at time t and equilibrium k_1 , and k_2 represent the first-order and second-order rate constants of adsorption, respectively.

The Eq. (3) for pseudo-first-order kinetics is plotted on a graph of $\ln(q_e - q_t)$ versus time (t) as shown in Fig. 8(a), a straight line is formed with a direction tangent of k_1 and an intersection point on the y axis of $\ln(q_e)$. The value of k_1 can be determined using linear regression. While Eq. (4) is represented in the t/q_t versus t graph as shown in Fig. 8(b), a straight line is produced with a direction tangent of $1/q_e$ and an intersection point on the y-axis of $1/k_2 q_e^2$. As a result, it is possible to determine the value of the constant k_2 .

In Table 1, kinetic information, adsorption rate constants, and regression coefficients are shown. The results demonstrated that CV adsorption by MRC and SRC had a pseudo-second-order kinetic model because the correlation coefficient (R^2) value was closer to 1, as we can see in Table 1. R^2 value on MRC 0.991 and SRC 0.982 [35]. The kinetic model obtained in this study is the same as several studies using carbon material as an adsorbent in the adsorption of CV [12,38-39].

If it is seen from the rate constant on the adsorbent, SRC is faster than MRC, inversely proportional to the percentage of adsorption obtained. These different rates

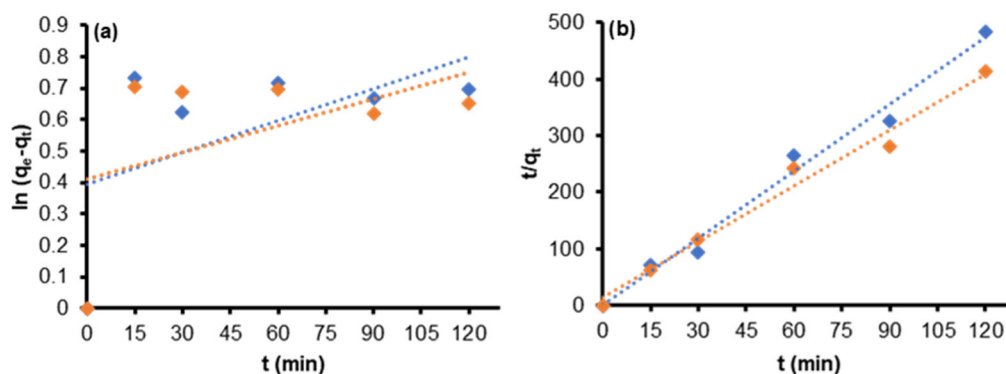


Fig 8. (a) Pseudo-first-order and (b) pseudo-second-order kinetics for adsorption of CV dye on MRC and SRC

Table 1. Kinetic parameters for CV adsorption on MRC and SRC

Adsorbents	Pseudo-first-order		Pseudo-second-order	
	k_1 (min^{-1}) (10^{-1})	R^2	k_2 ($\text{g mg}^{-1} \text{min}^{-1}$)	R^2
MRC	0.034	0.301	3.403	0.991
SRC	0.029	0.230	0.827	0.982

can be due to the presence of two active groups in SRC, namely (-OH) hydroxyl and (-C₆H₅) phenyl, so that it can carry out the adsorption process faster than MRC, which has an active group (-OH) in interacting with the active part of the dye, (N⁺) and the benzene ring. The fast adsorption time that lasts can affect the percentage of CV adsorption by the adsorbent.

Influence of Concentration and Adsorption Isotherm

The influence of CV adsorption concentration by MRC and SRC was carried out with various concentrations of 10, 25, 50, 75, 100, 150, 200, and 250 mg L⁻¹. The initial concentration used is plotted against the adsorption capacity (q) obtained, which can be seen in Fig. 7(d). The increase in initial concentration enhances the adsorption capacity of CV from 2.14 to 47.01 mg g⁻¹ for MRC adsorbent and from 2.27 to 54.63 mg g⁻¹ for SRC adsorbent. This increment is due to the adsorbent's high affinity, which enables the active site to adsorb the adsorbate better [12].

According to the statistics on adsorption capacity, MRC has a smaller adsorption capacity than SRC adsorbent. This fact can be explained due to the narrowing of the pores of the magnetite coating so that the surface's active site of the RC becomes slightly

reduced. MRC and SRC adsorbents can remove the CV dyes in the solution.

The result data of the influence of concentration were then analyzed using the Langmuir Eq. (5) and Freundlich adsorption isotherm pattern Eq. (6).

$$\frac{1}{q_e} = \frac{1}{q_m K_L C_e} + \frac{1}{q_m} \quad (5)$$

$$\log q_e = \log K_F + \frac{1}{n} \log C_e \quad (6)$$

where C_e (mg L⁻¹) is the equilibrium concentration of CV in solution, q_e (mg g⁻¹) is the equilibrium adsorption capacity, q_m is the adsorption capacity of a single layer, K_L (L mg⁻¹) is the equilibrium constant incorporating the binding site affinity, K_F ((mg g⁻¹)(L mg⁻¹)^{1/n}) is the adsorption capacity factor, and n is the adsorption intensity factor which has a value between 1 to 10 [35].

The linear plot equation C/m against C_e yields a straight line with $1/q_m K_L$ as the slope and $1/q_m$ as the intercept, which can be seen in Fig. 9(a). Hence, it may be used to determine K_L and q_m from the Langmuir equation. The linear plot of $\log q_e$ versus $\log C_e$ yields a straight line with $1/n$ as a slope and $\log K_F$ as an intercept, shown in Fig. 9(b). Therefore, the value of n and K_F can be determined.

The Langmuir isotherm model assumes that there are a certain number of active sites on the adsorbent's

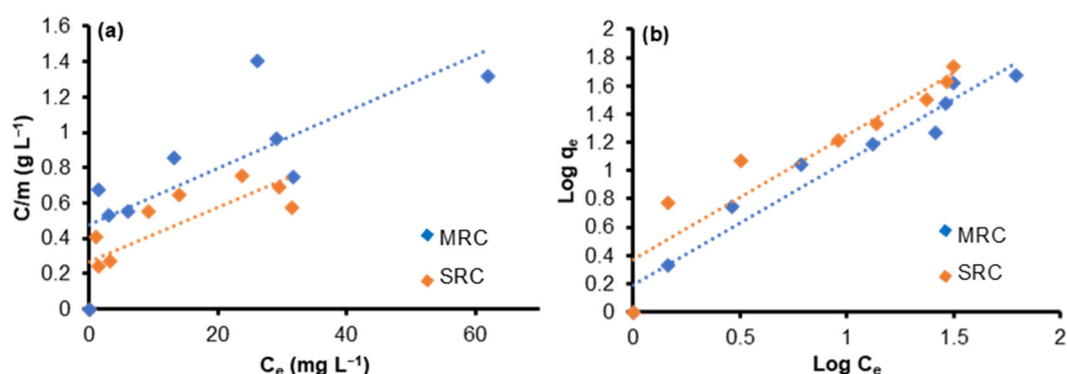


Fig 9. Adsorption isotherm of CV dye on MRC and SRC based on (a) Langmuir and (b) Freundlich

surface that are proportional to the surface area, the adsorbent surface is uniform, and the adsorption process is monolayer [40-41]. When the active site of a surface has been filled with adsorbate, there will be no additional adsorption at that site [42]. Thus, the maximum saturation point of adsorption on the adsorbent surface will be reached [43]. As a result, the occurrence of the adsorption process is known as monolayer adsorption. Freundlich's isotherm model is an empirical formula that is used to illustrate a heterogeneous system which is conveyed through Eq. (6) [44].

The Freundlich isotherm pattern tends to be followed in the adsorption of CV by MRC and SRC, as shown in Table 2. The Freundlich isotherm pattern of the adsorbent has a higher R^2 value than the Langmuir isotherm pattern, which is closer to 1. This fact

demonstrates that the adsorption occurs on a CV because not all of the adsorbent's active surfaces can do so; as a result, the adsorption that takes place is heterogeneous. The development of a multilayer on the surface of the adsorbent distinguishes the heterogeneous adsorption process [45].

The formation of layers on the surface of the adsorbent is caused by physical interactions that occur in the ongoing adsorption process [12]. Physical interactions that occur in CV adsorption by MRC and SRC can be in the form of electrostatic interactions between the hydroxyl group from Fe_3O_4 on MRC (Fig. 10(a)) and the hydroxyl group on SRC to the (N^+) group on the CV as well as π - π bond interactions between phenyl group on SRC to benzene ring on CV (Fig. 10(b)) [46-47].

Table 2. Isotherm parameters for adsorption of CV onto MRC and SRC

Adsorbents	Langmuir			Freundlich		
	q_m (mg g^{-1})	K_L (L mg^{-1})	R^2	n	K_F (mg g^{-1})(L mg^{-1}) $^{1/n}$)	R^2
MRC	71.429	0.025	0.428	1.093	1.362	0.943
SRC	69.930	0.049	0.549	1.026	1.761	0.932

Table 3. Comparison of MRC and SRC with other adsorbents used in CV removal

Adsorbent	q_m (mg g^{-1})	References
Rice husk activated carbon	11.18	[48]
AC- Fe_2O_3 .NPLs	16.50	[49]
ACL/ Fe_3O_4 magnetic nanocomposite	35.31	[39]
AC (Common Reed)	38.50	[50]
AC derived from Golbasi lignite	60.8–65.8	[51]
Chitosan AC	12.50	[16]
rGO/ Fe_3O_4 NCs	62.00	[52]
MRC (Rubber Fruit shell)	71.43	This Work
SRC (Rubber Fruit shell)	69.93	This Work

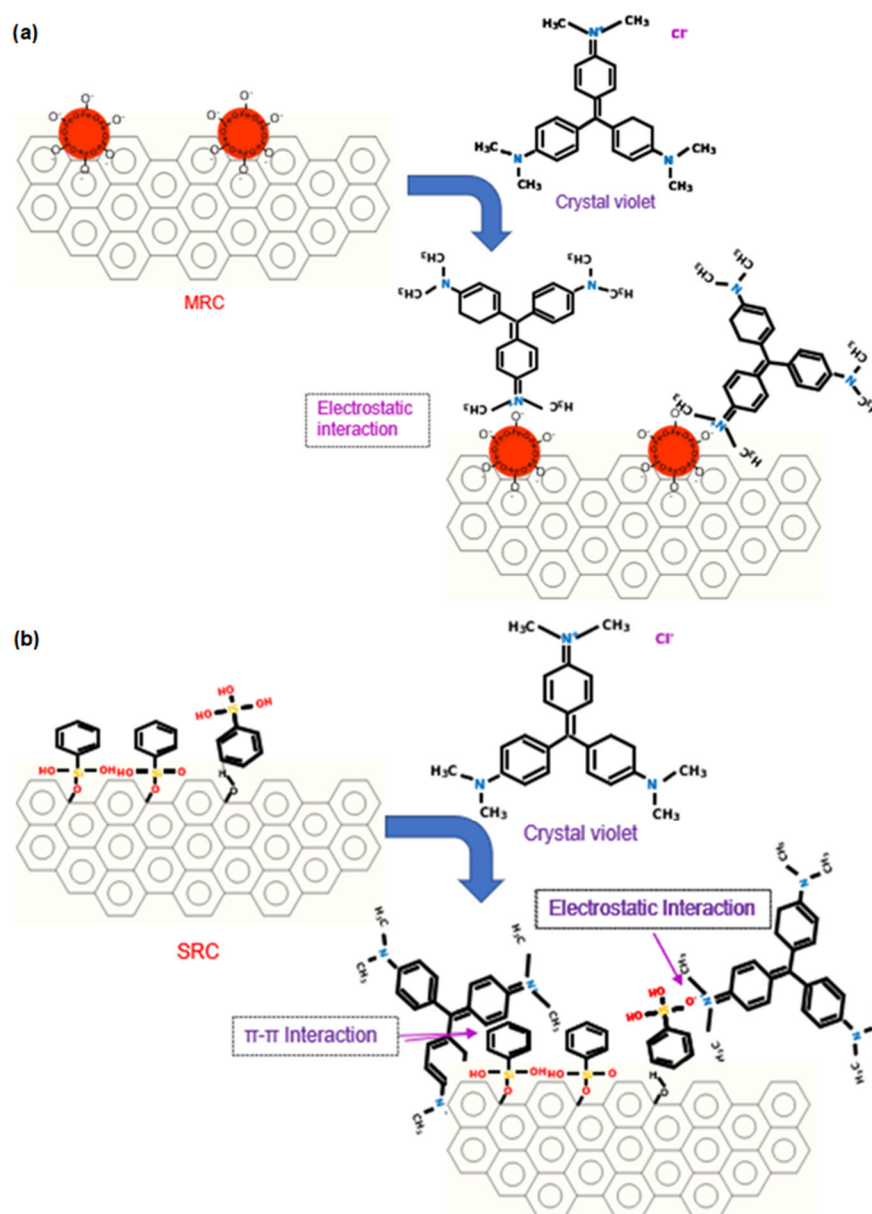


Fig 10. Mechanism adsorption of CV dye by (a) MRC and (b) SRC

If the adsorption capacity of the modified RC with magnetite and silane agents is compared with several adsorbents used to remove CV in solution (Table 3), it can be stated that MRC and SRC are effective adsorbents in absorbing CV. Thus, it can be stated that RC modification with magnetite coating and silane agent has increased the number of active adsorption sites on MRC and SRC. Our results align with the research reported by Alizadeh et al. [53], who used Azolla. Fig leaves modified magnetite nanoparticles as adsorbents in absorbing CV, and Jiao et

al. [54] used a hydrophobic clinoptilolite-modified silane coupling agent as a CV adsorption adsorbent.

CONCLUSION

In this research, modified RC with magnetite (MRC) and TEPS coupling agent (SRC) has been made, which is used as an effective and inexpensive adsorbent for CV dye solution. The adsorption capacity of MRC and SRC is influenced by several parameters, including adsorbent dose (0.1 g), pH (10), contact time (15 min),

and initial CV concentration (250 mg L^{-1}), with excellent results. The adsorption capacity obtained at MRC was 71.43, and SRC was 69.93 mg g^{-1} . The rate of adsorption kinetics tends to follow pseudo-second-order kinetics. The Freundlich isotherm is suitable for this adsorption compared to the Langmuir model, indicating that the adsorption that occurs is multilayer with physical interactions. MRC and SRC can be effective adsorbents to remove CV dye solution.

■ ACKNOWLEDGMENTS

The authors are grateful to the Research and Community Service Institute of the University of Lampung (LPPM Universitas Lampung) has funded this project with contract number: 819/UN26.21/PN/2022, and the Ministry of Education, Culture, Research, and Technology, Republic of Indonesia (Kemendikbud-Ristek) for the support of this research.

■ AUTHOR CONTRIBUTIONS

Nadya Syarifatul Fajriyah experimented. Nadya Syarifatul Fajriyah wrote the manuscript with the support and supervision of Buhani and Suharso. All authors approved the final version of the manuscript.

■ REFERENCES

- [1] Yahaya Sanda, B., and Ibrahim, I., 2020, Causes, categories and control of water pollution, *IJSES*, 4 (9), 84–90.
- [2] Foroutan, R., Peighambardoust, S.J., Aghdasinia, H., Mohammadi, R., and Ramavandi, B., 2020, Modification of bio-hydroxyapatite generated from waste poultry bone with MgO for purifying methyl violet-laden liquids, *Environ. Sci. Pollut. Res.*, 27 (35), 44218–44229.
- [3] Peighambardoust, S.J., Aghamohammadi-Bavil, O., Foroutan, R., and Arsalani, N., 2020, Removal of malachite green using carboxymethyl cellulose-g-polyacrylamide/montmorillonite nanocomposite hydrogel, *Int. J. Biol. Macromol.*, 159, 1122–1131.
- [4] Pashaei-Fakhri, S., Peighambardoust, S.J., Foroutan, R., Arsalani, N., and Ramavandi, B., 2021, Crystal violet dye sorption over acrylamide/graphene oxide bonded sodium alginate nanocomposite hydrogel, *Chemosphere*, 270, 129419.
- [5] Mittal, H., Al Alili, A., Morajkar, P.P., and Alhassan, S.M., 2021, Graphene oxide crosslinked hydrogel nanocomposites of xanthan gum for the adsorption of crystal violet dye, *J. Mol. Liq.*, 323, 115034.
- [6] Abdi, M., Balagabri, M., Karimi, H., Hossini, H., and Rastegar, S.O., 2020, Degradation of crystal violet (CV) from aqueous solutions using ozone, peroxone, electroperoxone, and electrolysis processes: A comparison study, *Appl. Water Sci.*, 10 (7), 168.
- [7] Thuong, N.T., Nhi, N.T.T., Nhung, V.T.C., Bich, H.N., Quynh, B.T.P., Bach, L.G., and Nguyen, T.D., 2019, A fixed-bed column study for removal of organic dyes from aqueous solution by pre-treated durian peel waste, *Indones. J. Chem.*, 19 (2), 486–494.
- [8] Thattil, P.P., and Rose, A.L., 2020, Enhanced removal of crystal violet dye using zinc oxide nanorods and air oxidation under sunlight radiation, *Rasayan J. Chem.*, 13 (2), 1166–1173.
- [9] Shi, B., Li, G., Wang, D., Feng, C., and Tang, H., 2007, Removal of direct dyes by coagulation: The performance of preformed polymeric aluminum species, *J. Hazard. Mater.*, 143 (1-2), 567–574.
- [10] Liu, H., Zhang, J., Lu, M., Liang, L., Zhang, H., and Wei, J., 2020, Biosynthesis based membrane filtration coupled with iron nanoparticles reduction process in removal of dyes, *Chem. Eng. J.*, 387, 124202.
- [11] Wu, J., Gao, H., Yao, S., Chen, L., Gao, Y., and Zhang, H., 2015, Degradation of crystal violet by catalytic ozonation using Fe/activated carbon catalyst, *Sep. Purif. Technol.*, 147, 179–185.
- [12] Buhani, B., Suharso, S., Luziana, F., Rilyanti, M., and Sumadi, S., 2019, Production of adsorbent from activated carbon of palm oil shells coated by Fe_3O_4 particle to remove crystal violet in water, *Desalin. Water Treat.*, 171, 281–293.
- [13] Permatasari, D., Buhani, B., Rilyanti, M., and

- Suharso, S., 2021, Adsorption kinetic and isotherm of solution pair of methylene blue and crystal violet by algae-silica-magnetite hybrid adsorbent on *Porphyridium* sp. algae, *J. Phys.: Conf. Ser.*, 1751, 012084.
- [14] Fabryanty, R., Valencia, C., Soetaredjo, F.E., Putro, J.N., Santoso, S.P., Kurniawan, A., Ju, Y.H., and Ismadji, S., 2017, Removal of crystal violet dye by adsorption using bentonite – alginate composite, *J. Environ. Chem. Eng.*, 5 (6), 5677–5687.
- [15] Ahmad, R., 2009, Studies on adsorption of crystal violet dye from aqueous solution onto coniferous pinus bark powder (CPBP), *J. Hazard. Mater.*, 171 (1-3), 767–773.
- [16] Jayasanthi Kumari, H., Krishnamoorthy, P., Arumugam, T.K., Radhakrishnan, S., and Vasudevan, D., 2017, An efficient removal of crystal violet dye from waste water by adsorption onto TLAC/Chitosan composite: A novel low cost adsorbent, *Int. J. Biol. Macromol.*, 96, 324–333.
- [17] Li, H., Qi, H., Yin, M., Chen, Y., Deng, Q., and Wang, S., 2021, Carbon tubes from biomass with prominent adsorption performance for paraquat, *Chemosphere*, 262, 127797.
- [18] Sebastian, A., Nangia, A., and Prasad, M.N.V., 2018, A green synthetic route to phenolics fabricated magnetite nanoparticles from coconut husk extract: Implications to treat metal contaminated water and heavy metal stress in *Oryza sativa* L., *J. Cleaner Prod.*, 174, 355–366.
- [19] Buhani, B., Hariyanti, F., Suharso, S., Rinawati, R., and Sumadi, S., 2019, Magnetized algae-silica hybrid from *Porphyridium* sp. biomass with Fe₃O₄ particle and its application as adsorbent for the removal of methylene blue from aqueous solution, *Desalin. Water Treat.*, 142, 331–340.
- [20] Singh, K.P., Gupta, S., Singh, A.K., and Sinha, S., 2011, Optimizing adsorption of crystal violet dye from water by magnetic nanocomposite using response surface modeling approach, *J. Hazard. Mater.*, 186 (2-3), 1462–1473.
- [21] Mohmood, I., Lopes, C.B., Lopes, I., Tavares, D.S., Soares, A.M.V.M., Duarte, A.C., Trindade, T., Ahmad, I., and Pereira, E., 2016, Remediation of mercury contaminated saltwater with functionalized silica coated magnetite nanoparticles, *Sci. Total Environ.*, 557-558, 712–721.
- [22] Buhani, B., Herasari, D., Suharso, S., and Yuwono, S.D., 2017, Correlation of ionic imprinting cavity sites on the amino-silica hybrid adsorbent with adsorption rate and capacity of Cd²⁺ ion in solution, *Orient. J. Chem.*, 33 (1), 418–429.
- [23] Zulaicha, A.S., Buhani, B., and Suharso, S., 2021, Modification of activated carbon from *Elaeis guineensis* Jacq shell with magnetite (Fe₃O₄) particles and study adsorption-desorption on Ni(II) ions in solution, *J. Phys.: Conf. Ser.*, 1751, 012086.
- [24] Wong, K.T., Yoon, Y., Snyder, S.A., and Jang, M., 2016, Phenyl-functionalized magnetic palm-based powdered activated carbon for the effective removal of selected pharmaceutical and endocrine-disruptive compounds, *Chemosphere*, 152, 71–80.
- [25] Kausar, R.A., Buhani, B., and Suharso, S., 2020, Methylene blue adsorption isotherm on *Spirulina* sp. microalgae biomass coated by silica-magnetite, *IOP Conf. Ser.: Mater. Sci. Eng.*, 857, 012019.
- [26] Buhani, B., Suharso, S., Rilyanti, M., Sari, M., and Sumadi, S., 2021, Removal of Cd(II) ions in solution by activated carbon from palm oil shells modified with magnetite, *Desalin. Water Treat.*, 218, 352–362.
- [27] Buhani, B., Suharso, S., Miftahza, N., Permatasari, D., and Sumadi, S., 2021, Improved adsorption capacity of *Nannochloropsis* sp. through modification with cetyltrimethylammonium bromide on the removal of methyl orange in solution, *Adsorpt. Sci. Technol.*, 2021, 1641074.
- [28] Yamaura, M., Camilo, R.L., Sampaio, L.C., Macêdo, M.A., Nakamura, M., and Toma, H.E., 2004, Preparation and characterization of (3-aminopropyl)triethoxysilane-coated magnetite nanoparticles, *J. Magn. Magn. Mater.*, 279 (2-3), 210–217.
- [29] Dalali, N., Habibzadeh, M., Rostamzadeh, K., and Nakisa, S., 2014, Synthesis of magnetite multi-

- walled carbon nanotubes composite and its application for removal of basic dyes from aqueous solutions, *Asia-Pac. J. Chem. Eng.*, 9 (4), 552–561.
- [30] Romanos, J., Beckner, M., Stalla, D., Tekeei, A., Suppes, G., Jalisatgi, S., Lee, M., Hawthorne, F., Robertson, J.D., Firlej, L., Kuchta, B., Wexler, C., Yu, P., and Pfeifer, P., 2013, Infrared study of boron-carbon chemical bonds in boron-doped activated carbon, *Carbon*, 54, 208–214.
- [31] Harimu, L., Wahyuni, S., Nasrudin, N., Baari, M.J., and Permana, D., 2022, Fabrication of chitosan/Fe₃O₄ nanocomposite as adsorbent for reduction methylene blue contents, *Indones. J. Chem.*, 22 (3), 878–886.
- [32] Khuluk, R.H., Rahmat, A., Buhani, B., and Suharso, S., 2019, Removal of methylene blue by adsorption onto activated carbon from coconut shell (*Cococus nucifera* L.), *Indones. J. Sci. Technol.*, 4 (2), 229–240.
- [33] Gundogdu, A., Duran, C., Senturk, H.B., Soylak, M., Ozdes, D., Serencam, H., and Imamoglu, M., 2012, Adsorption of phenol from aqueous solution on a low-cost activated carbon produced from tea industry waste: Equilibrium, kinetic, and thermodynamic study, *J. Chem. Eng. Data*, 57 (10), 2733–2743.
- [34] Mohan, D., Sarswat, A., Singh, V.K., Alexandre-Franco, M., and Pittman, C.U., 2011, Development of magnetic activated carbon from almond shells for trinitrophenol removal from water, *Chem. Eng. J.*, 172 (2-3), 1111–1125.
- [35] Buhani, B., Halimah, S.N., Suharso, S., and Sumadi, S., 2022, Utilization of activated carbon from candlenut shells (*Aleurites moluccana*) as methylene blue adsorbent, *Rasayan J. Chem.*, 15 (1), 124–131.
- [36] Singh, A., Kumar, S., Panghal, V., Arya, S.S., and Kumar, S., 2019, Utilization of unwanted terrestrial weeds for removal of dyes, *Rasayan J. Chem.*, 12 (4), 1956–1963.
- [37] Kakavandi, B., Jonidi Jafari, A., Rezaei Kalantary, R., Nasser, S., Esrafil, A., Gholizadeh, A., and Azari, A., 2016, Simultaneous adsorption of lead and aniline onto magnetically recoverable carbon: Optimization, modeling and mechanism, *J. Chem. Technol. Biotechnol.*, 91 (12), 3000–3010.
- [38] Abdel-Salam, A.H., Ewais, H.A., and Basaleh, A.S., 2017, Silver nanoparticles immobilised on the activated carbon as efficient adsorbent for removal of crystal violet dye from aqueous solutions. A kinetic study, *J. Mol. Liq.*, 248, 833–841.
- [39] Foroutan, R., Peighambar, S.J., Peighambar, S.H., Pateiro, M., and Lorenzo, J.M., 2021, Adsorption of crystal violet dye using activated carbon of lemon wood and activated carbon/Fe₃O₄ magnetic nanocomposite from aqueous solutions: A kinetic, equilibrium and thermodynamic study, *Molecules*, 26 (8), 2241.
- [40] Toan, N.C., Binh, Q.A., Tungtakanpoung, D., and Kajitvichyanukul, P., 2020, Kinetic, isotherm and mechanism in paraquat removal by adsorption processes using different biochars, *Lowl. Technol. Int.*, 22 (2), 304–317.
- [41] Iryani, A., Nur, H., Santoso, M., and Hartanto, D., 2020, Adsorption study of rhodamine B and methylene blue dyes with ZSM-5 directly synthesized from Bangka kaolin without organic template, *Indones. J. Chem.*, 20 (1), 130–140.
- [42] Damiyine, B., Guenbour, A., and Boussem, R., 2020, Comparative study on adsorption of cationic dye onto expanded perlite and natural clay, *Rasayan J. Chem.*, 13 (1), 448–463.
- [43] Pranoto, P., Purnawan, C., and Utami, T., 2018, Application of Bekonang clay and andisol soil composites as copper(II) metal ion adsorbent in metal crafts wastewater, *Rasayan J. Chem.*, 11 (1), 23–31.
- [44] Shao, Y., Zhou, L., Bao, C., Ma, J., Liu, M., and Wang, F., 2016, Magnetic responsive metal-organic frameworks nanosphere with core-shell structure for highly efficient removal of methylene blue, *Chem. Eng. J.*, 283, 1127–1136.
- [45] Buhani, B., Narsito, N., Nuryono, N., Kunarti, E.S., and Suharso, S., 2015, Adsorption competition of Cu(II) ion in ionic pair and multi-metal solution by ionic imprinted amino-silica hybrid adsorbent, *Desalin. Water Treat.*, 55 (5), 1240–1252.
- [46] Wong, K.T., Eu, N.C., Ibrahim, S., Kim, H., Yoon,

- Y., and Jang, M., 2016, Recyclable magnetite-loaded palm shell-waste based activated carbon for the effective removal of methylene blue from aqueous solution, *J. Cleaner Prod.*, 115, 337–342.
- [47] Abbas, M., Harrache, Z., and Trari, M., 2020, Mass-transfer processes in the adsorption of crystal violet by activated carbon derived from pomegranate peels: Kinetics and thermodynamic studies, *J. Eng. Fibers Fabr.*, 15, 1558925020919847.
- [48] Mohanty, K., Naidu, J.T., Meikap, B.C., and Biswas, M.N., 2006, Removal of crystal violet from wastewater by activated carbons prepared from rice husk, *Ind. Eng. Chem. Res.*, 45 (14), 5165–5171.
- [49] Hamidzadeh, S., Torabbeigi, M., and Shahtaheri, S.J., 2015, Removal of crystal violet from water by magnetically modified activated carbon and nanomagnetic iron oxide, *J. Environ. Health Sci. Eng.*, 13 (1), 8.
- [50] Shouman, M.A., and Rashwan, W.E., 2012, Studies on adsorption of basic dyes on activated carbon derived from *Phragmites australis* (common reed), *Univers. J. Environ. Res. Technol.*, 2 (3), 119–134.
- [51] Depci, T., Kul, A.R., Onal, Y., Disli, E., Alkan, S., and Turkmenoglu, Z.F., 2012, Adsorption of crystal violet from aqueous solution on activated carbon derived from Gölbaşı lignite, *Physicochem. Probl. Miner. Process.*, 48 (1), 253–270.
- [52] Kahsay, M.H., Belachew, N., Tadesse, A., and Basavaiah, K., 2020, Magnetite nanoparticle decorated reduced graphene oxide for adsorptive removal of crystal violet and antifungal activities, *RSC Adv.*, 10 (57), 34916–34927.
- [53] Alizadeh, N., Shariati, S., and Besharati, N., 2017, Adsorption of crystal violet and methylene blue on azolla and fig leaves modified with magnetite iron oxide nanoparticles, *Int. J. Environ. Res.*, 11 (2), 197–206.
- [54] Jiao, J., Sun, J., Ullah, R., Bai, S., and Zhai, C., 2020, One-step synthesis of hydrophobic clinoptilolite modified by silanization for the degradation of crystal violet dye in aqueous solution, *RSC Adv.*, 10 (38), 22809–22818.